A late diagenetic (syn-folding) magnetization carried by pyrrhotite: implications for paleomagnetic studies from magnetic iron sulphide-bearing sediments

Richard Weaver *, Andrew P. Roberts, Andrew J. Barker

School of Ocean and Earth Science, University of Southampton, Southampton Oceanography Centre, Southampton SO14 3ZH, UK

Abstract

Paleomagnetic, rock magnetic, and sedimentary micro-textural data from an early Miocene mudstone sequence exposed in Okhta River, Sakhalin, Russia, indicate the presence of pyrrhotite and magnetite at different stratigraphic levels. Sites that contain only magnetite have a reversed polarity characteristic remanent magnetization (ChRM) with a low-coercivity overprint, which coincides with the present-day geomagnetic field direction. Pyrrhotite-bearing sites have stable normal polarity ChRMs that are significantly different from the present-day field direction. After correction for bedding tilt, the ChRM data fail a reversals test. However, the normal polarity pyrrhotite ChRM directions become antipodal to the tilt-corrected magnetite ChRM directions and are consistent with the expected geocentric axial dipole field direction at the site latitude after 40% partial unfolding. These data suggest that the pyrrhotite magnetization was acquired during folding and after lock-in of the magnetite remanences. Electron microscope observations of polished sections indicate that fluid-associated halos surround iron sulphide nodules. Pyrrhotite is present in randomly oriented laths in and around the nodules, and the nodules do not appear to have been deformed by sediment compaction. This observation is consistent with a late diagenetic origin of pyrrhotite. Documentation of a late diagenetic magnetization in pyrrhotite-bearing sediments here, and in recent studies of greigite-bearing sediments, suggests that care should be taken to preclude a late origin of magnetic iron sulphides before using such sediments for geomagnetic studies where it is usually crucial to establish a syn-depositional magnetization. © 2002 Elsevier Science B.V. All rights reserved.

Keywords: diagenesis; greigite; magnetite; pyrrhotite; Sakhalin Russian Federation; magnetization

1. Introduction

The ferrimagnetic iron sulphide minerals, greigite (Fe_3S_4) and monoclinic pyrrhotite (Fe_7S_8), have been reported to carry stable magnetizations in a variety of marine and lacustrine sedimentary environments [1–12]. Greigite forms under anoxic conditions, where bacterial sulphate reduction provides H_2S that reacts with detrital iron minerals to ultimately produce pyrite (FeS_2) [13,14]. In general, limited availability of sulphate is favourable for greigite formation, whereas higher concentrations of sulphate favour the production of

* Corresponding author. Tel.: +44-23-8059-2011;
Fax: +44-23-8059-3059/305.
E-mail address: rweaver@mail.soc.soton.ac.uk (R. Weaver).

the more stable pyrite [14–16]. The formation of pyrrhotite in sediments is more unexpected because it is predicted to occur at pH > 11 [17], which is beyond the range of values expected for sedimentary pore waters [18]. However, in the case of extremely low sulphur activity it is possible for pyrrhotite to form in sediments [17]. Clear documentation of the presence of pyrrhotite in sediments suggests that this condition has sometimes been met [1,5,6,10,12]. Evidence of early diagenetic sulphidization reactions in reducing sedimentary environments has led to the conclusion, in many cases, that magnetic iron sulphide minerals formed during early burial and that they record a near-depositional chemical remanent magnetization (CRM) [1,4–7].

In contrast to interpretations of early diagenetic pyrrhotite and greigite formation, several recent studies reveal the presence of contradictory magnetic polarities, even in adjacent samples, in sediments containing ferrimagnetic iron sulphide minerals [8,10–12,19–21]. A recent study demonstrates that greigite may not always form as an early diagenetic precursor to pyrite; it can occur as a result of late diagenetic reactions [21]. Pyrrhotite has also recently been proposed as a late diagenetic phase in a model diagenetic pathway for the Trubi marls from Sicily [12], although the timing of formation of the late diagenetic iron sulphide could not be established. In this study, we present results from Sakhalin, Russia, where the existence of pyrrhotite and the timing of pyrrhotite formation in a marine sedimentary sequence can be constrained by paleomagnetic and rock magnetic data as well as by sedimentary petrography. These results are discussed in terms of their implications for studies of geomagnetic field behaviour from sediments containing magnetic iron sulphide minerals.

2. Geological setting

Sakhalin is located off the east coast of mainland Russia, north of Japan, on the western margin of the Okhotsk Sea (Fig. 1). The west Sakhalin/Tatar Strait basin, which was originally a fore-arc basin between the Sikhote Al'in volcanic belt

and the eastern Sakhalin accretionary complex [22–24], contains a thick succession of shallow marine Cretaceous and Cenozoic sediments. Folding of these sequences occurred in response to right-lateral strike–slip deformation along the Central Sakhalin Fault (Fig. 1) [25].

Paleomagnetic samples were taken from eight sites across a stratigraphic interval of ∼70 m in an early Miocene sequence of marine mudstones of the lower Nevel'sk Suite for a study of regional tectonics [26]. The sampled sediments dip uniformly toward the west (21°W/182°) and are freshly exposed along Okhta River in southwest Sakhalin (Fig. 1). The marine mudstones consist of feldspar-rich siliciclastic material with a composition and texture that indicates a provenance from local igneous sources [23]. The location of the sampled sequence is shown in Fig. 1, along with a simplified stratigraphic column for southwest Sakhalin.

3. Methods

Oriented cylindrical paleomagnetic samples (10.8 cm^3) were collected in the field and the natural remanent magnetization (NRM) was measured using a 2G-Enterprises cryogenic magnetometer at the Southampton Oceanography Centre (SOC). Stepwise tumbling alternating field (AF) demagnetization was performed on the majority of samples using a Molspin AF demagnetizer because thermal demagnetization of pilot samples produced magnetic mineral alterations at elevated temperatures. For stably magnetized samples, AF and thermal demagnetization yielded similar results. AF demagnetization was preferred since the samples could be used for subsequent rock magnetic experiments. Characteristic remanent magnetization (ChRM) directions were identified from vector-component diagrams using principal component analysis [27]. ChRM directions were then analyzed using the statistics of Fisher [28].

Low-temperature magnetic measurements were conducted to identify possible magnetic transitions, which are diagnostic of magnetic mineralogy (e.g. [29–35]). A Quantum Design Magnetic Properties Measurement System (MPMS-XL5)

was used at the Institute for Rock Magnetism (IRM), Minneapolis, MN, USA. Usually, three different measurement cycles were carried out for samples from each site. A zero-field-cooled (ZFC) cycle was applied first, where the samples were cooled from 300 to 10 K in zero field. A saturation isothermal remanent magnetization (SIRM) was imparted using a 2.5 T field, which was switched off before measuring the SIRM at 5 K steps during warming back to 300 K. A field-cooled (FC) cycle was then applied, by cooling samples from 300 to 10 K in a 2.5 T field. The field was then switched off at 10 K and the magnetization measured at 5 K intervals during warming back to 300 K. Finally, a room temperature SIRM (RT-SIRM) cycle was applied, by imparting a 2.5 T SIRM at 300 K before switching off the field and measuring the magnetization at 5 K steps during cooling to 20 K and during warming back to 300 K.

Magnetic hysteresis loops and first-order reversal curve (FORC) diagrams [36] were acquired to assess the coercivity distributions of the magnetic assemblages in the samples. Measurements were made using a Princeton Measurements Corporation vibrating sample magnetometer at the IRM, with maximum applied fields of 1 T. Measured hysteresis parameters include: M_r (saturation remanence), M_s (saturation magnetization), H_c (coercive force), and H_{cr} (coercivity of remanence). The instrument is sufficiently sensitive to enable acquisition of high-quality data from relatively weak magnetic bulk samples (sensitivity = 10^{-9} Am^2).

High-temperature magnetic behaviour was investigated using a variable field translation balance at the SOC. An applied field of 76 mT was used and the magnetization was measured during heating at 10°C/min from RT to 700°C and during cooling back to RT. Measurements were all carried out in air because iron sulphides are thermally unstable and use of inert atmospheres can give rise to variable rates of thermal alteration and less diagnostic thermomagnetic behaviour
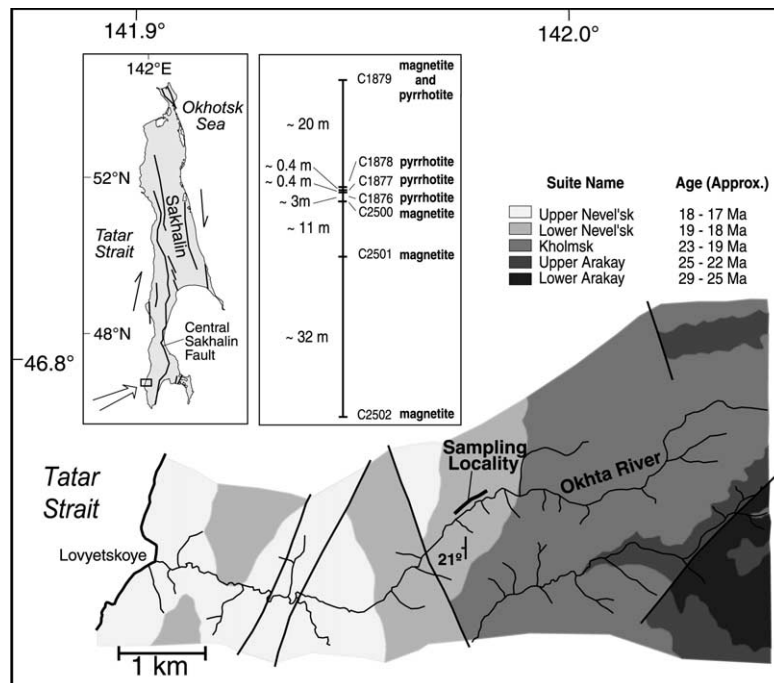

Fig. 1. Location map of Okhta River, SW Sakhalin, with simplified geological map, summary stratigraphic section for the sampled interval, and magnetic mineralogy at each sampled site. Approximate ages and mapped geological units are from an unpublished map provided by V. Galversen, Sakhalin Geological Expedition.

[37]. Thermal demagnetization of three-axis IRMs [38] was carried out to determine the magnetic minerals in different coercivity components. Fields of 0.9, 0.3 and 0.12 T were applied to representative samples, along the x, y and z axes, respectively.

Sediment micro-textures were studied in polished thin sections from representative samples using a LEO 1450VP scanning electron microscope (SEM) operated at 15 keV at the SOC. Elemental analyses were obtained from energy-dispersive X-ray spectra (EDS) generated from point analyses (2–3 μm beam diameter) of individual mineral grains, using a Princeton Gamma Tech (IMIX-PTS) system. X-ray diffraction (XRD) patterns were obtained using a Philips X-ray diffractometer (CoKα radiation) at the SOC to identify minerals.

4. Results

4.1. Rock magnetism

Of the eight sites sampled at the Okhta River section, one is unstably magnetized, three are dominated by magnetite, three are dominated by pyrrhotite, and one has magnetic properties con-

Table 1
Paleomagnetic data from Okhta River, Sakhalin

Sample	In situ		100% untilted		40% untilted		Error	In situ	
	Dec. (°)	Inc. (°)	Dec. (°)	Inc. (°)	Dec. (°)	Inc. (°)	MAD (°)	Dec. (°)	Inc. (°)
Magnetite								Overprint	
C2500/2	227.2	−57.6	189.9	−67.6	–	–	3.3	329.8	80.7
C2500/3	229.4	−58.2	191.3	−68.8	–	–	3.9	0.0	65.7
C2500/4	234.7	−60.5	192.2	−72.3	–	–	2.5	330.1	77.8
C2501/2	224.3	−55.5	190.2	−64.9	–	–	5.5	27.6	72.6
C2501/3	212.6	−59.8	172.8	−64.0	–	–	4.9	339.7	70.3
C2501/4	217.5	−57.4	180.8	−63.9	–	–	7.0	3.6	63.7
C2502/1	177.0	−63.4	175.4	−70.4	–	–	22.8	294.9	54.8
C2502/3	204.4	−62.2	162.6	−62.8	–	–	10.1	–	–
C2502/4	203.6	−55.6	171.1	−57.7	–	–	16.2	346.1	73.9
Mean	215.4	−59.9	179.7	−66.2					
α_{95}	5.8		4.0						
Magnetite and pyrrhotite									
C1879/1	39.1	62.8	350.7	67.8	359.2	68.2	2.6	348.2	60.6
C1879/2	35.4	63.4	348.4	67.4	9.3	65.7	2.1	351.6	62.5
C1879/3	38.3	62.7	349.8	66.9	14.9	66.2	0.6	21.7	64.5
C1879/4	18.3	69.8	321.7	61.9	337.1	59.7	6.1	–	–
Mean								348.5	70.0
α_{95}								7.2	
Pyrrhotite									
C1876/1	42.0	75.0	322.7	72.5	4.9	76.5	4.3	–	–
C1876/2	23.3	60.9	330.0	63.9	351.0	69.4	10.3	–	–
C1876/3	39.2	72.7	326.5	67.3	357.1	71.6	5.5	–	–
C1877/1	14.9	67.1	332.2	60.3	354.9	65.8	10.0	–	–
C1877/3	2.1	78.3	315.6	66.0	7.3	71.1	4.7	–	–
C1877/4	25.1	72.0	329.3	68.0	0.4	69.1	3.6	–	–
C1878/1	29.9	64.1	343.2	65.9	11.0	67.0	7.9	–	–
C1878/2	9.8	60.6	334.9	56.8	353.3	59.9	6.2	–	–
C1878/3	17.4	68.2	328.1	64.4	351.1	69.6	7.1	–	–
Mean	26.2	67.9	333.4	65.7	358.7	68.0			
α_{95}	3.7		3.1		3.1				

Bedding: 21°W/182°; MAD: maximum angular deviation for analyzed vector components; α_{95}: 95% confidence limit for the mean paleomagnetic direction. The mean pyrrhotite direction includes magnetite and pyrrhotite data.

sistent with a mixture of magnetite and pyrrhotite (Table 1). In the following discussion, we present results from each of these groups in turn.

Vector-component diagrams from sites C2500-C2502 reveal a two-component NRM after AF demagnetization (Fig. 2a,b). The low-coercivity magnetic component (0–20 mT) has normal polarity. A ChRM component with reversed polarity is present between the 25 and 60 mT. The demagnetization trajectory suggests minimal overlap of the two components. The same ChRM component appears in thermally demagnetized samples, although the data are noisier (Fig. 2b). The NRM is almost removed at 550°C, which suggests that low-titanium magnetite is present (Fig. 2b). Low-temperature thermomagnetic curves contain evidence of a weak Verwey transition at ∼ 120 K, as suggested by a small peak in the plot of the derivative of the magnetic moment with respect to temperature, which confirms the presence of mag-

netite (Fig. 2c). The weak nature of the transition may result from surficial oxidation of the magnetite [39]. Magnetic hysteresis parameters were determined for a bulk sediment sample (Fig. 2d) and FORC diagrams have contours that close around a peak at $H_c = 28$ mT with little vertical spread of the contours (Fig. 2e). This coercivity value is consistent with the presence of single domain (SD) magnetite and lack of vertical spread of the contours suggests that interactions among magnetite particles is negligible [36]. Divergent contours that intersect the H_u axis indicate a fraction of multidomain (MD) or pseudo SD grains. An additional small peak around the origin of the FORC diagram indicates that superparamagnetic (SP) grains are present [36,40]. Considered together, the rock magnetic evidence suggests that non-interacting magnetite, with a broad distribution of grain sizes, is the main magnetic mineral at these sites.
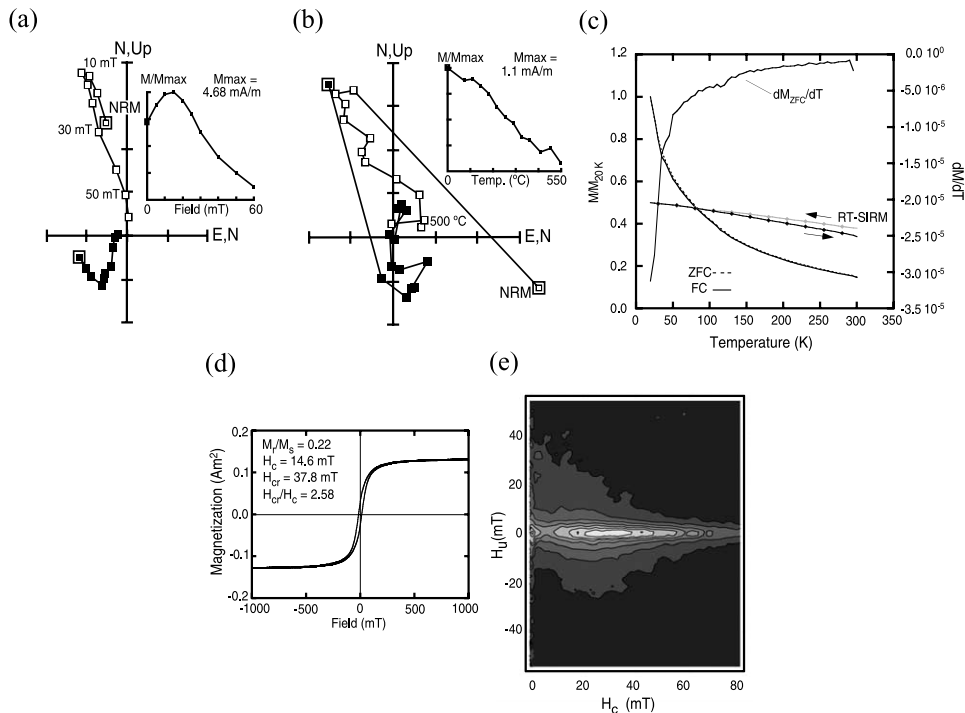

Fig. 2. Representative rock magnetic data for sites C2500–2502. Typical vector-component diagrams for (a) AF demagnetization (sample C2500/3), and (b) thermal demagnetization (sample C2502/1). Open symbols indicate paleomagnetic inclinations and solid symbols indicate paleomagnetic declinations. The inset graphs show the decay of magnetization during stepwise demagnetization. (c) Normalized low-temperature ZFC, FC and RT-SIRM curves (sample C2500/4). The first derivative of the ZFC curve is also plotted. (d) Hysteresis loop with associated hysteresis parameters (sample C2500/3). (e) FORC diagram (sample C2500/3).

Contrasting rock magnetic characteristics are observed for sites C1876–1878, which are situated higher in the sedimentary sequence than sites C2500–2502 (Fig. 1). Vector-component diagrams typically display a single normal polarity remanence component, which appears to be stable at AFs up to 80 mT (Fig. 3a). Thermal demagnetization indicates rapid thermal decay of the same component up to around 280°C, where thermal alteration starts to occur (Fig. 3b). Low-temperature magnetic transitions are not clearly evident in the ZFC, FC or RT-SIRM curves, although there is a small anomaly in the derivative of magnetization with respect to temperature and a separation of the ZFC and FC curves at around 30–40 K for samples from site C1878 (Fig. 3c).

The magnetic ordering temperature for siderite ($FeCO_3$) at 38 K [34] and a magnetic transition for pyrrhotite (34 K) are known to occur in this temperature range [29,30], so this anomaly is not necessarily indicative of the presence of pyrrhotite. However, observed coercivity of remanence values of 68.4 mT (Fig. 3d), are similar to those reported for ferrimagnetic iron sulphides such as greigite or pyrrhotite [10,30,33,41–43]. FORC diagrams suggest that high-coercivity ($H_c \approx 60$ mT) SD particles are present with relatively strong magnetic interactions between particles (Fig. 3e) [36]. High-temperature measurements conducted on strongly magnetic iron sulphide nodules that were manually extracted from the bulk sediment undergo a steep drop in magnetization between
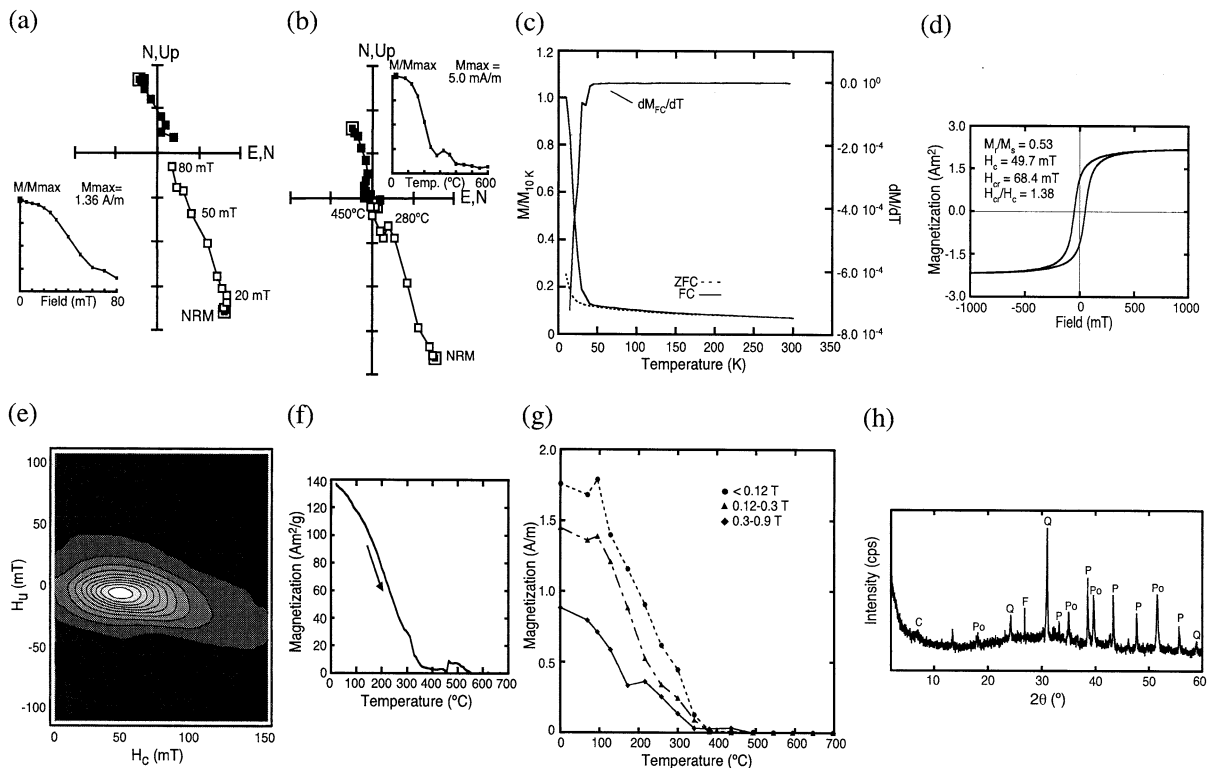

Fig. 3. Representative rock magnetic and mineralogical data for sites C1876-C1878. Typical vector-component diagrams for (a) AF demagnetization (sample C1877/1), and (b) thermal demagnetization (sample C1876/4). Symbols are the same as in Fig. 2. (c) Normalized low-temperature ZFC and FC curves (sample C1877/4). (d) Hysteresis loop with associated hysteresis parameters (sample C1877/1). (e) FORC diagram (sample C1877/1). (f) High-temperature thermomagnetic curve from extracted iron sulphide nodule (sample C1877/1). (g) Thermal demagnetization of three-axis IRM (sample C1877/1). (h) XRD analysis for a manually extracted iron sulphide nodule prior to heating. C = clay, Po = pyrrhotite, Q = quartz, F = feldspar, and P = pyrite.

150°C and 300°C, with thermal alteration to form magnetite above 400°C (Fig. 3f). The heating curve decreases sharply at ∼320°C, which likely indicates the presence of monoclinic pyrrhotite ($T_c = 320$°C), before falling to near-zero magnetizations at 350°C (Fig. 3f). Mineral alteration at higher temperatures probably results from trace amounts of clay minerals or pyrite altering to form magnetite (e.g. [1,10,12,43,44]). Thermal demagnetization of a three-axis IRM indicates a sharp decrease of magnetization between 140 and 300°C for all three components before reaching near-zero values at ∼340°C (Fig. 3g). The maximum unblocking temperature and range of coercivities suggest that monoclinic pyrrhotite is present [38]. Finally, XRD data from an iron sulphide nodule sample, analyzed prior to heating, contain strong pyrrhotite peaks (Fig. 3h). Addi-

tional peaks for pyrite, quartz, clays and feldspar are identified. There is no evidence for magnetite or greigite at these sites.

Higher in the studied sequence, a relatively soft magnetization component (< 50 mT) is isolated with a stable ChRM direction similar to the pyrrhotite-bearing sites described above (Fig. 4a). ZFC and FC curves separate at 30–40 K (Fig. 4b) and there is a small anomaly in the derivative, which suggests that pyrrhotite may be present [29,30]. Hysteresis loops from bulk samples yield coercivities that are intermediate between the magnetite- and pyrrhotite-bearing sites (Fig. 4c). The nature of the magnetic mineral assemblage is more clearly apparent in FORC diagrams (Fig. 4d), where contours close around a SD peak at $H_c = 25$–30 mT, with a small SP peak about the origin of the plot similar to that for the magne-
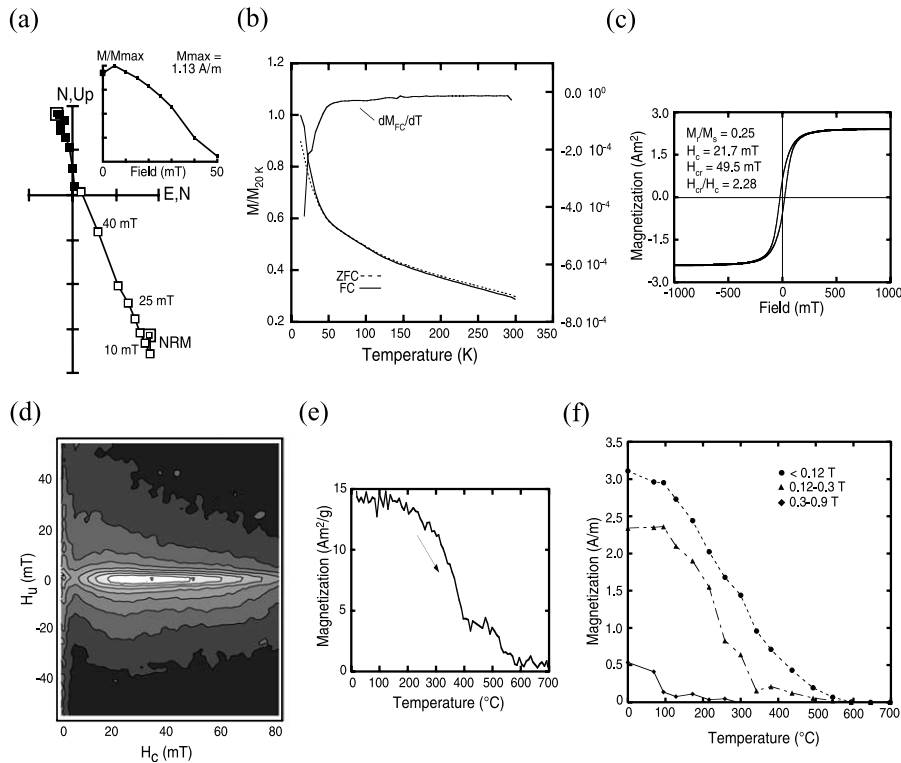

Fig. 4. Representative rock magnetic data for site C1879. (a) Vector-component diagram for AF demagnetization (sample C1879/3). Symbols are the same as in Fig. 2. (b) Normalized low-temperature ZFC and FC curves (sample C1879/3). (c) Hysteresis loop with associated hysteresis parameters (sample C1879/1). (d) FORC diagram (sample C1879/1). (e) High-temperature thermomagnetic curve (sample C1879/3). (f) Thermal demagnetization of three-axis IRM (sample C1879/1).

tite-bearing sample at site C2500 (Fig. 2e). Comparison of the FORC diagrams in Figs. 2e and 4d highlights some important differences. Equivalent contours extend to higher coercivities (e.g. 70 mT compared to 60 mT) and the vertical spread is somewhat greater in Fig. 4d. Both observations suggest that pyrrhotite occurs in addition to a broad range of magnetite grain sizes at this site. The high-temperature magnetization of the bulk sediment is characterized by a steep decrease between 300 and 400°C and alteration to form magnetite occurs above 400°C (Fig. 4e), which is typical of iron sulphide-bearing sediments [33,44]. The hard IRM component reduces to zero at around 300°C, while thermal demagnetization of the intermediate and soft IRM components indicates a steep decrease between 160 and 340°C before decaying more slowly to zero at 550–600°C (Fig. 4f). FORC distributions that are smeared toward higher coercivities, sharp decreases in magnetization at around 300–400°C, interactions between magnetic particles, and persistence of a magnetic component up to 580°C, suggest a mixed magnetic mineral assemblage where magnetite and pyrrhotite co-exist. The ChRM is probably carried by pyrrhotite (because of directional agreement with other pyrrhotite-bearing sites as described below). As is the case for the magnetite-only sites, the magnetite is likely to be present in a wide range of sizes from SP to MD sizes. The presence of a MD magnetite fraction could also explain the lack of a clear separa-

tion between ZFC and FC curves at temperatures below 120 K [31].

The stratigraphic relationship between the analyzed sites is shown in Fig. 1, with a summary of the magnetic minerals identified at each site. Hysteresis ratios from each site are plotted in Fig. 5. Samples containing pyrrhotite yield mostly SD-like data ($M_r/M_s > 0.5$, $H_{cr}/H_c \approx 1.5$), while magnetite-bearing samples tend toward values of $M_r/M_s \approx 0.2$ and $H_{cr}/H_c \approx 2.5$–3.0. Data from samples with a mixed magnetic mineral assemblage plot along a mixing line between the magnetite and pyrrhotite end-members (Fig. 5). This is consistent with the rock magnetic observations described above.

4.2. Paleomagnetism

Analysis of paleomagnetic directions was carried out before and after correction for bedding tilt. Normal polarity directions are associated with samples containing pyrrhotite (Fig. 3a,b) and stable reversed polarity ChRM directions are found in samples containing magnetite (Fig. 2a,b). In pre-tilt (in situ) coordinates, the mean direction for the magnetite-only samples is: $D = 215.4°$, $I = -59.9°$, with $\alpha_{95} = 5.8°$ (Table 1). The mean in situ direction for the pyrrhotite-bearing samples is: $D = 26.2°$, $I = 67.9°$, with $\alpha_{95} = 3.7°$ (Fig. 6a; Table 1). Low-coercivity magnetic overprints, identified in all of the magnetite-bearing samples and in some of the mixed pyrrhotite+magnetite samples, have a mean pre-tilt direction of: $D = 348.5°$, $I = 70.0°$, with $\alpha_{95} = 7.2°$ (Fig. 6b; Table 1). This direction is similar to the present-day field direction at the locality (IGRF, $D = 349.5°$, $I = 61.2°$ [45]). After applying a full tilt correction (21°W/182°) to the ChRM data, the mean directions for each group are not antipodal and therefore fail a reversals test [45]. Pyrrhotite-bearing samples plot about a mean of: $D = 333.4°$, $I = 65.7°$, with $\alpha_{95} = 3.1°$ (Table 1). The magnetite samples are indistinguishable from the expected geocentric axial dipole (GAD) direction for a Miocene reversed polarity field at the site latitude [26]: $D = 179.7°$, $I = -66.2°$, with $\alpha_{95} = 4.0°$ (Fig. 6c; Table 1). The normal polarity paleomagnetic data from the pyrrhotite-bearing
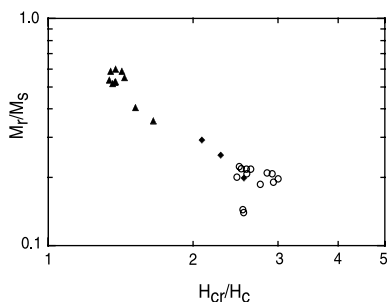

Fig. 5. Hysteresis parameters (M_r/M_s vs. H_{cr}/H_c) for sites from Okhta River. Open circles indicate magnetite-bearing samples, solid diamonds indicate samples containing pyrrhotite and magnetite, and solid triangles indicate samples containing pyrrhotite.
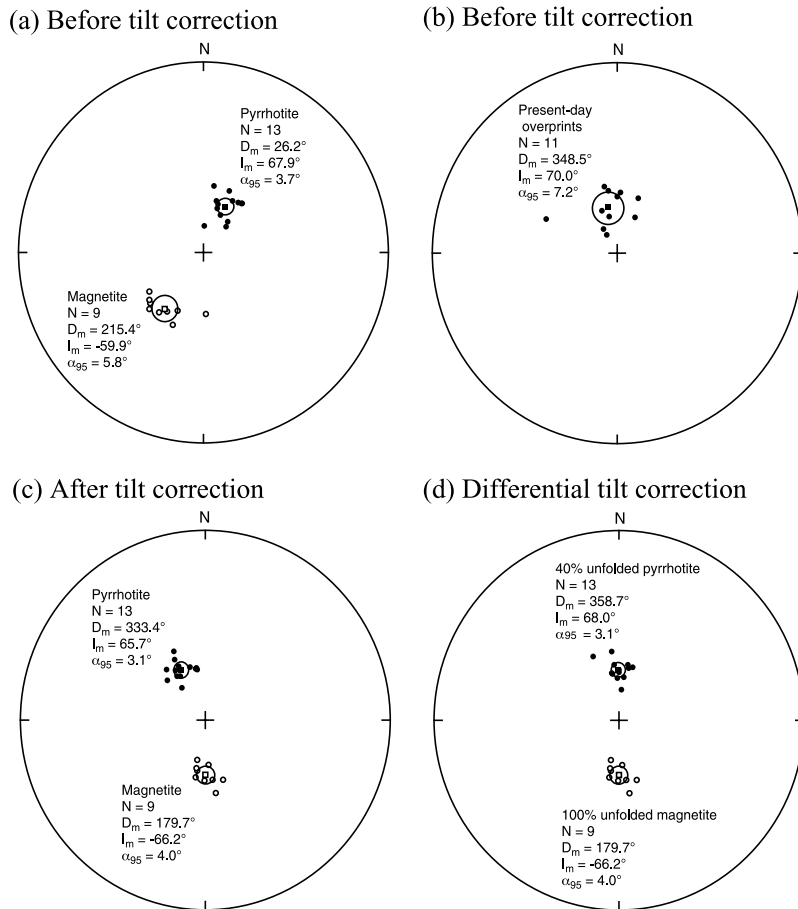
Fig. 6. Equal-area stereographic projections (lower hemisphere) of paleomagnetic data with mean directions indicated by a square. Solid symbols indicate normal polarity and open symbols indicate reversed polarity. The mean paleomagnetic directions are accompanied by 95% confidence ellipses.

samples are neither consistent with an expected GAD direction nor with the present-day field direction. The pyrrhotite data only become antipodal to the fully corrected magnetite direction at 40% untilting. After this partial unfolding, the pyrrhotite directions align with the expected GAD field direction, with: $D = 358.7°$, $I = 68.0°$, and $\alpha_{95} = 3.1°$ (Fig. 6d; Table 1).

4.3. Electron microscopy

Polished thin sections from samples containing pyrrhotite, magnetite and mixtures of both minerals were analyzed using a SEM with EDS. Ferrimagnetic iron sulphides are usually associated with pyrite in sediments deposited under anoxic conditions [14,15]. Pyrite and pyrrhotite can be distinguished under the SEM, because pyrrhotite has a greater molecular mass and should therefore appear brighter than pyrite in backscattered electron images. In addition, EDS spectra indicate a significantly larger difference between iron and sulphur peaks for pyrite than for pyrrhotite (Fig. 7a,b).

Pyrite is abundant in all samples. It is most easily identified in polished sections as round framboids that consist of aggregates of small crystals. Isolated pyrite framboids occur in the sediment matrix, but usually they appear in clusters (Fig. 7c,d). The larger framboids are about 10 μm
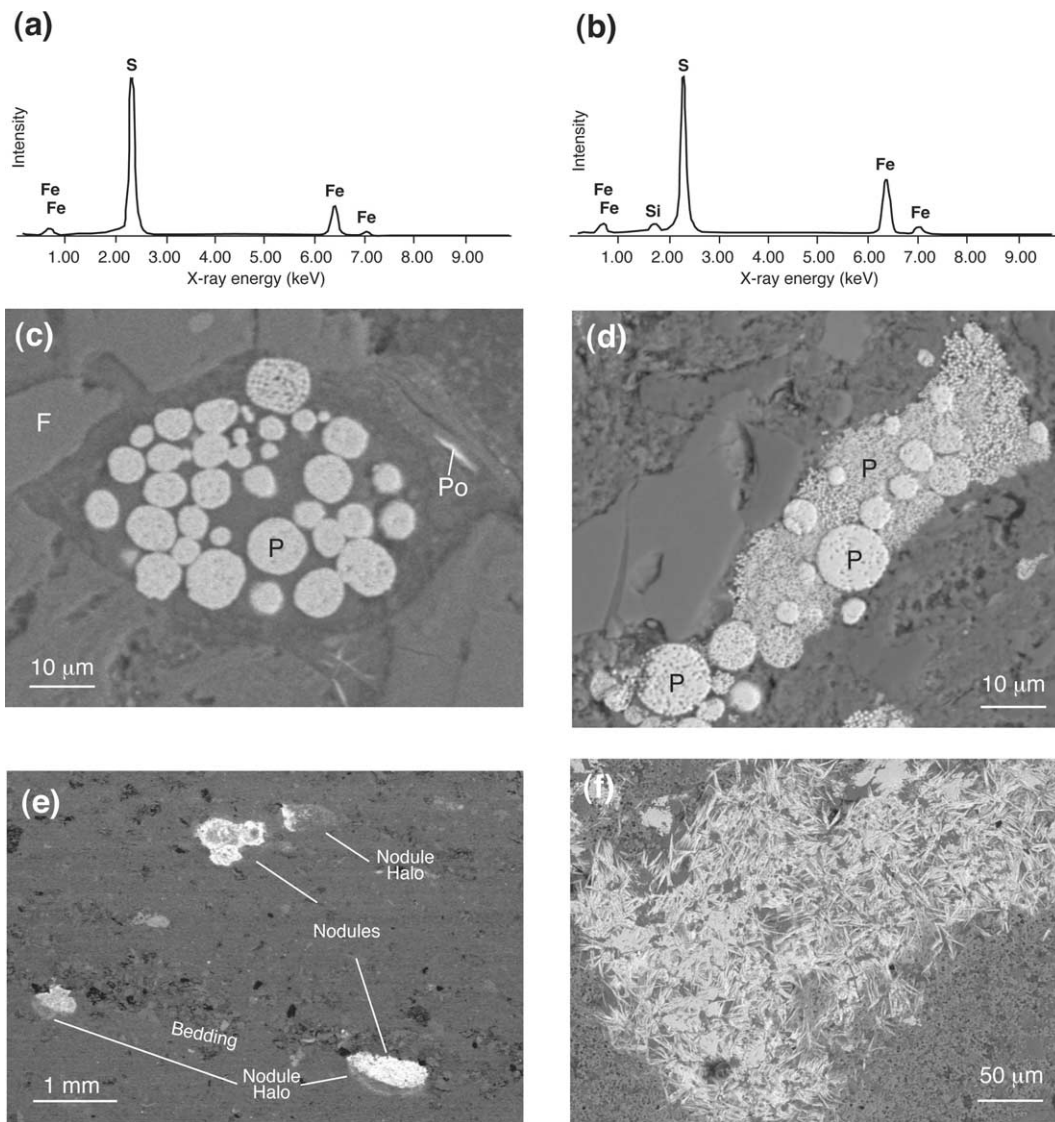
Fig. 7. X-ray energy-dispersive spectra for (a) pyrite and (b) pyrrhotite. Backscattered electron micrographs for (c) spherical pyrite framboids (P) arranged in groups on the surface and around the edges of detrital silicate minerals. Pyrrhotite (Po) is identified in the cleavage of a mica grain (sample C1979/1). (d) Polyframboidal pyrite (P) aggregate where later growth of pyrite appears to have occurred between larger framboids (sample C2501/3). (e) Overview of iron sulphide nodules in the overall context of the sediment matrix (sample C1877/1). (f) Higher magnification of a typical iron sulphide nodule consisting of pyrrhotite laths with no preferred orientations (sample C1878/3).

in diameter. In pyrrhotite-bearing samples, clustered pyrite framboids are usually separated from each other (Fig. 7c). Pyrrhotite sometimes occurs as growths into micro-cracks in the matrix, often in the vicinity of pyrite framboid aggregates (Fig. 7c). In magnetite-only samples, the interstices between framboids are filled with aggregates of pyrite crystals (Fig. 7d); no magnetic iron sulphides were observed.

The main mode of occurrence of pyrrhotite in the pyrrhotite-bearing samples is in iron sulphide nodules. These nodules (up to about 2 mm) have
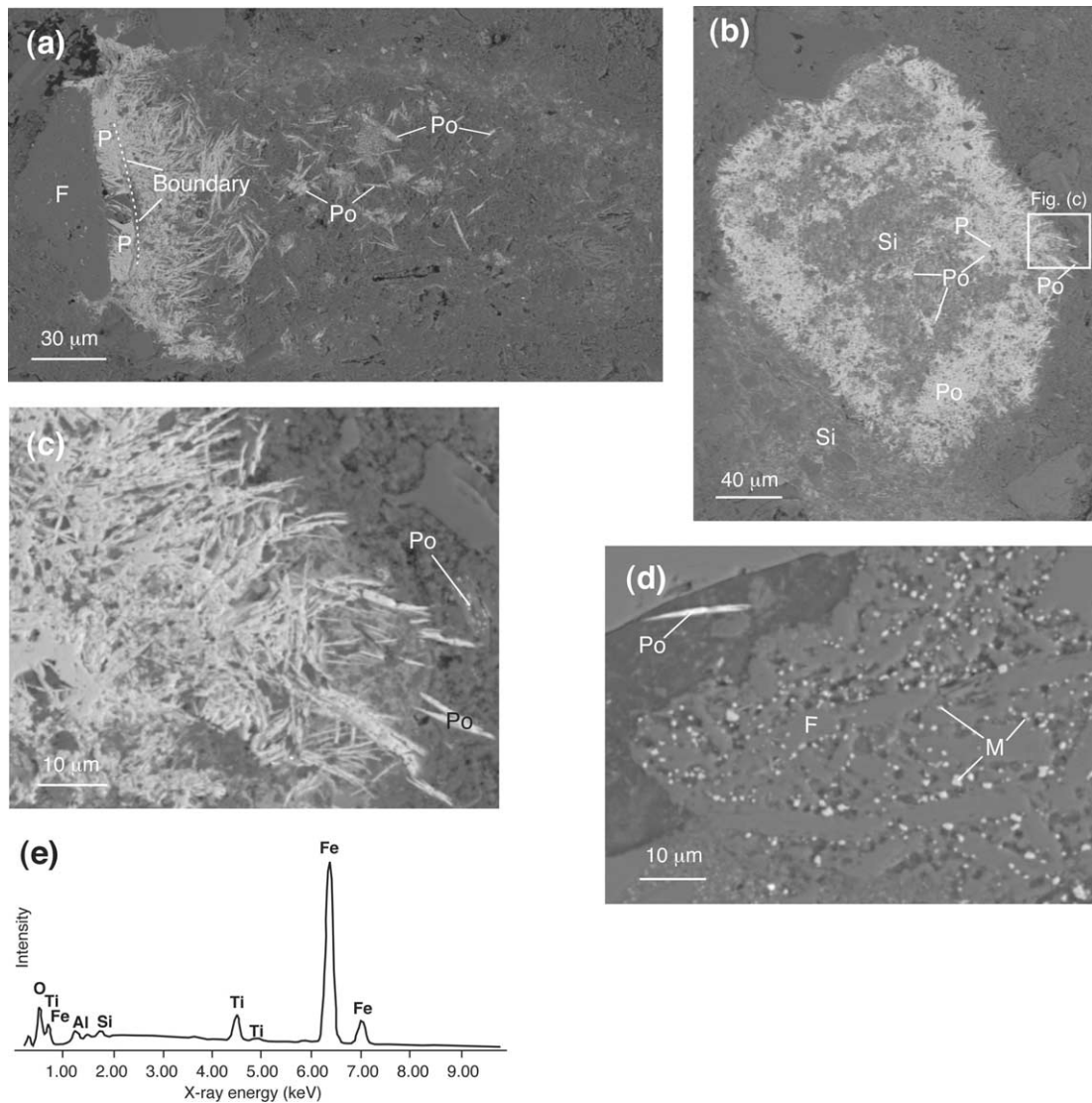
Fig. 8. Backscattered electron micrographs. (a) Pyrrhotite nodule with a halo in the shadow of a feldspar (F) grain. Pyrite (P) is identified close to the right-hand grain boundary. Away from the boundary, pyrrhotite (Po) is dominant in fibrous laths (sample C1877/1). (b) Acicular pyrrhotite (Po) exists around the edges of a mass of silica (Si). Larger crystals of pyrite (P) are found in the center of the nodule (sample C1877/1). (c) High-magnification reveals the presence of small pyrrhotite (Po) grains along micro-cleavage planes in mica grains close to large nodules (sample C1877/1). (d) Submicron magnetite particles (M) occur within large detrital feldspathic (F) clasts (sample C1879/1). (e) EDS of (Ti-) magnetite particles within feldspathic clasts.

variable shape and occur with distinctive halos surrounding them (Fig. 7e). At higher magnifications, the nodules have a fibrous or spiky exterior surface, comprising a dense mass of randomly oriented fine acicular laths (Fig. 7f). SEM–EDS analyses consistently indicate a pyrrhotite composition, which corroborate XRD analyses on the same nodules (Fig. 3h). Similar fibrous laths have been reported for other occurrences of pyrrhotite in sediments [12,46]. In addition, pyrite is found in the nodules, but it tends to occur as larger grains in contrast to its framboidal appearance elsewhere in the sediment matrix.

Nodular masses of pyrrhotite laths and pyrite

seem to occur in variable contexts (Fig. 8a,b). In one case, pyrite can be identified as tightly clustered laths along the edge of a large feldspar crystal. They are oriented at a high angle to the feldspar surface and extend up to 15 μm from this surface. There is an apparent boundary in the matrix, beyond which the needles consist of pyrrhotite. The pyrrhotite crystals appear to be randomly oriented and become progressively less dense with distance from the feldspar crystal edge (Fig. 8a).

In another case, pyrite and acicular pyrrhotite are found around the edges, and in patches within a mass of silica (Fig. 8b). Pyrite is also found as a smooth tabular area toward the edge of the silica mass, whereas pyrrhotite occurs as a mesh of interlocking needles and also along the (001) cleavage of mica grains in peripheral regions of the silica mass (Fig. 8c).

Fine magnetite particles are not evident in the nodular pyrrhotite-bearing samples. In the magnetite-bearing samples, magnetite particles are difficult to detect because of their small (submicron) size. In the sample containing pyrrhotite and magnetite, the magnetite occurs as small interstitial grains between feldspar crystals within felsic volcanic clasts (Fig. 8d). Small amounts of titanium are usually present in the magnetite (Fig. 8e).

5. Discussion

5.1. Paleomagnetic evidence for a syn-folding magnetization in pyrrhotite

Tectonically corrected ChRM data from sites with normal polarity (pyrrhotite samples) and reversed polarity (magnetite-only samples) have mean directions that are not antipodal and the data consequently fail a reversals test (Fig. 6c). The mean declination of the normal polarity overprints is in good agreement with the present-day field direction (IGRF, $D = 349.5°$, $I = 61.2°$ [45]), although the inclination of the overprint is steeper than the IGRF direction. The directional precision of the overprint may have been affected by the later exposure of samples to laboratory fields.

The overprint (Fig. 6b) is probably a viscous remanent magnetization that resides in fine magnetite particles near the SP/SD grain-size boundary, as indicated by the presence of a secondary peak near the origin of FORC diagrams (Figs. 2e and 4d). The pre-tilt corrected normal polarity pyrrhotite component has a direction that is different from the overprint, with a clockwise-deflected declination of 26.2° (Fig. 6a). Clearly, the normal polarity ChRM associated with pyrrhotite cannot have originated from remagnetization in the present-day field. When data from magnetite-bearing sites are corrected for stratal tilt, a reversed polarity direction that is consistent with a GAD field at the site latitude is obtained (Fig. 6c). It is therefore clear that the pyrrhotite ChRM data are anomalous: they neither record a pre-folding GAD direction nor a post-folding present-day field direction. Differential unfolding of data from the two groups of sites, with the magnetite data fully unfolded and the pyrrhotite data subjected to 40% unfolding, reveals antipodal directions (Fig. 6d). The resultant mean directions are consistent with the expected time-averaged GAD field for the site latitude ($D = 0°$, $I = 65°$) [26]. The data suggest that a CRM has been acquired by the pyrrhotite, which post-dates the magnetite ChRM directions, and which appears to be a syn-folding magnetization.

5.2. Micro-textural evidence for the timing of nodular iron sulphide formation

Different textures of iron sulphides in the Okhta River samples give clues about the timing of their formation. Groups of pyrite framboids with clear spaces between them suggest a relatively early stage of formation (cf. [16]). Groups of pyrite framboids are found in all of the studied sites (Fig. 7c,d). In the magnetite-bearing sediments, interstitial voids are filled by polyframboidal pyrite aggregates (Fig. 7d) [47]. This process requires abundant sulphate for ongoing pyritization. No ferrimagnetic iron sulphides are evident in the magnetite-bearing samples. Thus, although the magnetite-bearing site has clearly undergone early diagenetic sulphidization, these reactions have neither led to the complete dissolution of magne-

tite nor to the preservation of magnetic iron sulphides.

While early diagenetic pyrite framboids are ubiquitous in all of the sites analyzed here, late diagenetic magnetizations are only observed in samples containing iron sulphide nodules (Figs. 7e,f and 8). Non-framboidal pyrite crystals are present within these nodules (Fig. 8a,b). The nodules, which dominantly consist of acicular pyrrhotite laths, are well-defined within the sediment matrix (Fig. 7e) and do not display any preferred orientation. The morphology of the non-framboidal elongate pyrite is similar to the pyrrhotite (Fig. 8a), which suggests that pyrite has locally replaced pyrrhotite. Furthermore, the acicular pyrrhotite crystals appear to have random orientations and do not show any signs of deformation around the edges of nodules due to sediment compaction. These observations suggest that the nodules formed after sediment compaction [48].

Fluid flow is likely to be associated with the formation of the nodules. The nodules usually have halos around them which define regions where diagenetic fluid/mineral interactions may have taken place (Figs. 7e and 8a,b). This is particularly apparent in Fig. 8a, where a small iron sulphide nodule is asymmetrically developed on one side of a feldspar grain. The morphology of the feldspar crystal appears to have controlled the nodule shape and the distribution of iron sulphides, which would be possible by restricting or deviating a sulphidic fluid around it. It is conceivable that the feldspar crystal provided an impermeable barrier to the fluid which was forced to flow around the grain, and that the fluid migrated down a localized fluid pressure gradient caused by a dilating micro-crack at the feldspar–matrix interface. Pyrrhotite then nucleated on the feldspar surface to form lath-like or acicular crystals, later to be replaced by pyrite (Fig. 8a). Since these crystals are at a high angle to the feldspar surface, it suggests face-controlled growth into a dilating micro-crack rather than growth by replacement. Less sulphidic fluid appears to have permeated further to the right of the boundary, to produce acicular pyrrhotite crystals in the adjacent matrix. A halo has formed to the right of the feldspar crystal and seems to mark the limits of possible sulphidic fluid migration and the associated distribution of pyrrhotite. Another nodule has silica in its core and within the alteration halo below the nodule (Fig. 8b). The nodule is dominated by pyrrhotite laths toward the outside, with some larger pyrite crystals toward the center. In the cases shown in Fig. 8a,b, there are chemical iron sulphide gradients associated with the nodules, which may be linked with fluid flow. The halo textures seem to be diagnostic of the presence of a diagenetic fluid and it seems that differences in chemical gradients for iron and sulphur have resulted in different iron sulphide products (pyrite or pyrrhotite), which have a determining control on the magnetization of the sediment.

The overall micro-textural evidence from pyrrhotite nodules (especially randomly oriented laths) suggests a late diagenetic formation that post-dates sediment compaction. All of the samples that contain pyrrhotite, as indicated by rock magnetic and XRD analyses, also contain nodules that can be identified in hand specimen and using SEM observations. Magnetostatic interactions between particles, as suggested by the vertical spread in FORC distributions (Fig. 3e), are consistent with microscopic evidence for the closely intergrown nature of the pyrrhotite laths in the iron sulphide nodules.

At site C1879, where magnetite and pyrrhotite co-exist (Fig. 1; Table 1), magnetite occurs as abundant submicron interstitial grains within (> 40 μm) clasts of felsic volcanic rock (Fig. 8d), which are relatively common in samples from this site. They appear to be randomly oriented, which probably explains why the magnetite does not appear to be paleomagnetically significant at this site and why the ChRM is dominated by pyrrhotite.

5.3. Implications for paleomagnetism

Chemical remagnetization of sediments associated with late diagenetic iron sulphide minerals is being increasingly documented [8,10–12,19–21,37]. Our data suggest that the magnetization in the studied sediments was acquired during folding and that a tectonically driven fluid migration event has altered the redox conditions to enable

late diagenetic growth of pyrrhotite. Tightly-clustered remanence directions from the pyrrhotite-bearing sites suggests that the pyrrhotite formed within a relatively short period of time, which is consistent with a CRM due to a fluid-activated event of limited duration. It is only possible to speculate about the source of fluid that allowed the chemical reaction to occur. Late diagenetic magnetizations carried by iron sulphide minerals could be linked to numerous processes including the migration of hydrocarbons, gas hydrates, hydrothermal fluids or release of trapped pore waters [49–52]. Alternatively, slow reactions in sulphate-limited environments might enable late diagenetic formation of magnetic iron sulphide phases [21]. Climatic or regional tectonic forcing can also alter the redox conditions in sedimentary basins, which may allow authigenic iron sulphides to form. It is clear that great care is needed to assess the origin of the magnetic remanence in order to establish a reliable timing for magnetizations carried by magnetic iron sulphide minerals.

Late diagenetic (syn-folding) acquisition of a CRM in pyrrhotite has been demonstrated in this study and suggests that the assumption of early diagenetic remanence acquisition in magnetic iron sulphide-bearing sediments may not be appropriate for studies of short-term geomagnetic field behaviour such as secular variation or geomagnetic polarity transitions (e.g. [1,4]). In addition to fine-scale field behaviour, the magnetic polarity record of a sedimentary sequence can be compromised by late CRM acquisition, as has recently been documented in several cases [8,10–12,20]. It should be noted, however, that in one case where greigite and pyrrhotite are both present, the greigite usually carried a late diagenetic signal whereas the pyrrhotite carried a syn-depositional signal [10].

Depending on the timing of remanence acquisition, an iron sulphide CRM could also be difficult to interpret in tectonic studies. In cases where there have been multiple phases of deformation, lack of knowledge of the exact timing of remanence acquisition could prove particularly confusing. In particular, careful consideration should be given to the formation processes of the magnetic iron sulphide to ensure that geomagnetic secular variation can be properly averaged. Field tests are of paramount importance to evaluate whether a magnetic iron sulphide carries a primary CRM (e.g. fold test, reversals test, conglomerate test).

6. Conclusions

Paleomagnetic data from a marine mudstone sequence sampled at Okhta River, Sakhalin, suggest that the magnetization is a syn-folding CRM carried by pyrrhotite. Rock magnetic and XRD results confirm the presence of pyrrhotite and SEM analyses indicate that the pyrrhotite dominantly occurs in nodules in the studied samples. The nodules consist of pyrrhotite laths that have no preferred orientation and which show no evidence of deformation during sediment compaction. This suggests that the nodules formed after sediment compaction. Halos around the nodules suggest that fluids have played an important part in the formation of the pyrrhotite nodules. Together, the paleomagnetic, rock magnetic, and micro-textural evidence suggests that pyrrhotite formed during late diagenesis in association with a tectonically driven fluid migration event.

The documented late diagenetic magnetizations carried by pyrrhotite do not give a reliable syn-depositional paleomagnetic signal, which is required for detailed studies of geomagnetic field behaviour. Geological, environmental and oceanographic events are also likely to be misinterpreted from polarity records based on a CRM carried by magnetic iron sulphide minerals unless the timing of remanence acquisition can be accurately constrained. In tectonic studies where the deformation is multiphase and complex, it is critical that the mean paleomagnetic direction represents a time-averaged direction that predates deformation. It is clear from this study that a great deal of care must be taken to establish the timing of remanence acquisition in studies of magnetic iron sulphide-bearing sediments.

References

[1] J.H. Linssen, Preliminary results of a study of four successive sedimentary geomagnetic reversal records from the Mediterranean (Upper Thvera, Lower and Upper Sidufjall, and Lower Nunivak), Phys. Earth Planet. Inter. 52 (1988) 207–231.

[2] I.F. Snowball, R. Thompson, A stable chemical remanence in Holocene sediments, J. Geophys. Res. 95 (1990) 4471–4479.

[3] V. Kalcheva, P. Nozharov, M. Kovacheva, V. Shopov, Paleomagnetic research on Black Sea Quaternary sediments, Phys. Earth Planet. Inter. 63 (1990) 113–120.

[4] E. Tric, C. Laj, C. Jehanno, J.-P. Valet, C. Kissel, A. Mazaud, S. Iaccarino, High-resolution record of the Upper Olduvai transition from Po Valley (Italy) sediments: support for dipolar transition geometry?, Phys. Earth Planet. Inter. 65 (1991) 319–336.

[5] C. Mary, S. Iaccarino, V. Courtillot, J. Besse, D.M. Aïssaoui, Magnetostratigraphy of Pliocene sediments from the Stirone River (Po Valley), Geophys. J. Int. 112 (1993) 359–380.

[6] A.P. Roberts, G.M. Turner, Diagenetic formation of ferrimagnetic iron sulphide minerals in rapidly deposited marine sediments, South Island, New Zealand, Earth Planet. Sci. Lett. 115 (1993) 257–273.

[7] D.F. Hallam, B.A. Maher, A record of reversed polarity carried by the iron sulphide greigite in British early Pleistocene sediments, Earth Planet. Sci Lett. 121 (1994) 71–80.

[8] F. Florindo, L. Sagnotti, Palaeomagnetism and rock magnetism in the upper Pliocene Valle Ricca (Rome, Italy) section, Geophys. J. Int. 123 (1995) 340–354.

[9] A.P. Roberts, R.L. Reynolds, K.L. Verosub, D.P. Adam, Environmental magnetic implications of greigite (Fe_3S_4) formation in a 3 m.y. lake sediment record from Butte Valley, northern California, Geophys. Res. Lett. 23 (1996) 2859–2862.

[10] C.-S. Horng, M. Torii, K.-S. Shea, S.-J. Kao, Inconsistent magnetic polarities between greigite- and pyrrhotite/magnetite-bearing marine sediments from the Tsailiao-chi section, southwestern Taiwan, Earth Planet. Sci. Lett. 164 (1998) 467–481.

[11] C. Richter, A.P. Roberts, J.S. Stoner, L.D. Benning, C.T. Chi, Magnetostratigraphy of Pliocene-Pleistocene sediments from the eastern Mediterranean Sea, Proc. ODP Sci. Res. 160 (1998) 61–74.

[12] J. Dinarès-Turell, M.J. Dekkers, Diagenesis and remanence acquisition in the Lower Pliocene Trubi marls at Punta di Maiata (southern Sicily): palaeomagnetic and rock magnetic observations, in: D.H. Tarling, P. Turner (Eds.), Palaeomagnetism and Diagenesis in Sediments, Geol. Soc. Lond. Spec. Publ. 151, 1999, pp. 53–69.

[13] R.A. Berner, Sedimentary pyrite formation, Am. J. Sci. 268 (1970) 1–23.

[14] R.A. Berner, Sedimentary pyrite formation: an update, Geochim. Cosmochim. Acta 48 (1984) 605–615.

[15] R.E. Sweeney, I.R. Kaplan, Pyrite framboid formation: laboratory synthesis and marine sediments, Econ. Geol. 68 (1973) 618–634.

[16] R.T. Wilkin, H.L. Barnes, Formation processes of framboidal pyrite, Geochim. Cosmochim. Acta 61 (1997) 323–339.

[17] R.M. Garrels, C.L. Christ, Solutions, Minerals and Equilibria, Harper and Row, New York, 1965, 450 pp.

[18] W. Stumm, J.J. Morgan, Aquatic Chemistry (2nd edn.), Wiley and Sons, 1981, 780 pp.

[19] W. Xu, R. VanderVoo, D. Peacor, Electron microscopic and rock magnetic study of remagnetized Leadville carbonates, central Colorado, Tectonophysics 296 (1998) 333–362.

[20] R. Thompson, T.J.D. Cameron, Palaeomagnetic study of Cenozoic sediments in North Sea boreholes: an example of a magnetostratigraphic conundrum in a hydrocarbon-producing area, in: P. Turner, A. Turner (Eds.), Palaeomagnetic Applications in Hydrocarbon Exploration, Geol. Soc. Lond. Spec. Publ. 98, 1995, pp. 223–236.

[21] W.-T. Jiang, C.-S. Horng, A.P. Roberts, D.R. Peacor, Contradictory magnetic polarities in sediments and variable timing of neoformation of authigenic greigite, Earth Planet. Sci. Lett. 193 (2001) 1–12.

[22] G. Kimura, The latest Cretaceous-early Paleogene rapid growth of accretionary complex and exhumation of high pressure series metamorphic rocks in northwestern Pacific margin, J. Geophys. Res. 99 (1994) 22147–22164.

[23] L.P. Zonenshain, M.I. Kuz'min, L.V. Natapov, Geology of the USSR: a plate tectonic synthesis, in: B.M. Page (Ed.), AGU Geodynamic Series 21, Washington, DC, 1990.

[24] V.S. Zyabrev, N.Y. Bragin, Deep water terrigeneous sedimentation in the West Sakhalin Trough, Dokl. Akad. Nauk SSSR 292 (1987) 168–171.

[25] V.S. Rozhdestvenskiy, The role of wrench-faults in the structure of Sakhalin, Geotectonics 16 (1982) 323–332.

[26] R. Weaver, A.P. Roberts, R. Flecker, D.I.M. Macdonald,

L.M. Fot'yanova, Geodynamic implications of paleomagnetic data from Tertiary sediments in Sakhalin, Russia (NW Pacific), J. Geophys. Res., (2002) in press.

[27] J.L. Kirschvink, The least-squares line and plane analysis of palaeomagnetic data, Geophys. J. R. Astron. Soc. 62 (1980) 699–718.

[28] R.A. Fisher, Dispersion on a sphere, Proc. R. Soc. Lond. 217 (1953) 295–305.

[29] M.J. Dekkers, J.-L. Mattéi, G. Fillion, P. Rochette, Grain-size dependence of the magnetic behaviour of pyrrhotite during its low-temperature transition at 34 K, Geophys. Res. Lett. 16 (1989) 855–858.

[30] P. Rochette, G. Fillion, J.-L. Mattéi, M.J. Dekkers, Magnetic transition at 30–34 Kelvin in pyrrhotite: insight into a widespread occurrence of this mineral in rocks, Earth Planet. Sci. Lett. 98 (1990) 319–328.

[31] B.M. Moskowitz, R.B. Frankel, D.A. Bazylinski, Rock magnetic criteria for the detection of biogenic magnetite, Earth Planet. Sci. Lett. 120 (1993) 283–300.

[32] B.M. Moskowitz, M. Jackson, C. Kissel, Low-temperature magnetic behaviour of titanomagnetites, Earth Planet. Sci. Lett. 157 (1998) 141–149.

[33] A.P. Roberts, Magnetic properties of sedimentary greigite (Fe_3S_4), Earth Planet. Sci. Lett. 134 (1995) 227–236.

[34] B.A. Housen, S.K. Banerjee, B.M. Moskowitz, Low-temperature magnetic properties of siderite and magnetite in marine sediments, Geophys. Res. Lett. 23 (1996) 2843–2846.

[35] M. Torii, K. Fukuma, C.-S. Horng, T.-Q. Lee, Magnetic discrimination of pyrrhotite- and greigite-bearing sediment samples, Geophys. Res. Lett. 23 (1996) 1813–1816.

[36] A.P. Roberts, C.R. Pike, K.L. Verosub, First-order reversal curve diagrams: a new tool for characterizing the magnetic properties of natural samples, J. Geophys. Res. 105 (2000) 28461–28475.

[37] R.L. Reynolds, M.L. Tuttle, C.A. Rice, N.S. Fishman, J.A. Karachewski, D.M. Sherman, Magnetization and geochemistry of greigite-bearing Cretaceous strata, North Slope Basin, Alaska, Am. J. Sci. 294 (1994) 485–528.

[38] W. Lowrie, Identification of ferromagnetic minerals in a rock by coercivity and unblocking temperature properties, Geophys. Res. Lett. 17 (1990) 159–162.

[39] Ö. Özdemir, D.J. Dunlop, B.M. Moskowitz, The effect of oxidation on the Verwey transition in magnetite, Geophys. Res. Lett. 20 (1993) 1671–1674.

[40] C.R. Pike, A.P. Roberts, K.L. Verosub, First-order reversal curve diagrams and thermal relaxation effects in magnetic particles, Geophys. J. Int. 145 (2001) 721–730.

[41] M.J. Dekkers, Magnetic properties of natural pyrrhotite. I. Behaviour of initial susceptibility and saturation-magnetization-related rock magnetic parameters in a grain-size-dependent framework, Phys. Earth Planet. Inter. 52 (1988) 376–393.

[42] I.F. Snowball, Magnetic hysteresis properties of greigite (Fe_3S_4) and a new occurrence in Holocene sediments from Swedish Lappland, Phys. Earth Planet. Inter. 68 (1991) 32–40.

[43] L. Sagnotti, A. Winkler, Rock magnetism and palaeomagnetism of greigite-bearing mudstones in the Italian peninsula, Earth Planet. Sci. Lett. 165 (1999) 67–80.

[44] M.J. Dekkers, Magnetic monitoring of pyrrhotite alteration during thermal demagnetization, Geophys. Res. Lett. 17 (1990) 779–782.

[45] L. Tauxe, Paleomagnetic Principles and Practice, Kluwer Academic, 1998, pp. 299.

[46] R.L. Reynolds, M.B. Goldhaber, M.L. Tuttle, Sulphidization and magnetization above hydrocarbon reservoirs, in: D.J. Aïssaoui, D.F. McNeil, N.F. Hurley (Eds.), Applications of Paleomagnetism to Sedimentary Geology, SEPM Spec. Publ. 49, 1993, pp. 167–179.

[47] L.G. Love, Early diagenetic polyframboidal pyrite, primary and redeposited, from the Wenlockian Denbigh Grit group, Conway, north Wales, UK, J. Sediment. Petrol. 41 (1971) 1038–1044.

[48] J. Sellés-Martínez, Concretion morphology, classification and genesis, Earth Sci. Rev. 41 (1996) 177–210.

[49] H.G. Machel, E.A. Burton, Causes and spatial distribution of anomalous magnetization in hydrocarbon seepage environments, Am. Assoc. Petrol. Geol. Bull. 75 (1991) 1864–1876.

[50] R.L. Reynolds, R.S. Fishman, M.R. Hudson, Sources of aeromagnetic anomalies over Cement oil field (Alaska), and the Wyoming-Idaho-Utah thrust belt, Geophysics 56 (1991) 606–617.

[51] B.A. Housen, R.J. Musgrave, Rock-magnetic signature of gas hydrates in accretionary prism sediments, Earth Planet. Sci. Lett. 139 (1996) 509–519.

[52] M. Urbat, M.J. Dekkers, K. Krumsiek, Discharge of hydrothermal fluids through sediment at the Escanaba Trough, Gorda Ridge (ODP Leg 169): assessing the effects on the rock magnetic signal, Earth Planet. Sci. Lett. 176 (2000) 481–494.